A Temperature- and Molar Mass-Dependent Change in the Crystallization Mechanism of Poly(1-butene): Transition from Chain-Folded to Chain-Extended Crystallization?

Qiang Fu,*,†,‡ B. Heck,‡ G. Strobl,‡ and Y. Thomann§

Department of Polymer Science and Materials, Sichuan University, Chengdu 610065, China; Fakultät für Physik der Albert-Ludwigs-Universität, 79104 Freiburg, Germany; and Institut für Makromolekulare Chemie der Albert-Ludwigs-Universität, 79104 Freiburg, Germany

Received September 14, 2000; Revised Manuscript Received December 11, 2000

ABSTRACT: The crystallization behavior of poly(1-butene) (P1b) was investigated by polarized light microscopy (PLM), atomic force microscopy (AFM), wide-angle X-ray scattering (WAXS), dilatometry, and also by time- and temperature-resolved small-angle X-ray scattering experiments (SAXS). Observations in the PLM indicate a temperature-dependent change in the mechanism of crystallization. When crossing a certain critical crystallization temperature, the morphology changes from spherulites to quadratic, platelike single crystals. Investigations of samples with different molar mass show that the transition temperature is molar mass-dependent; on decreasing the molar mass the transition shifts to lower temperatures. As proved by WAXS, both the spherulites and the single crystals are of the metastable form II. The morphological change is also observed in AFM images obtained after a rapid cooling of the samples to room temperature; the difference in the morphological appearance is preserved through the transformation from form II to form I. According to dilatometric measurements, the change in the crystallization mechanism leads to variations in the temperature dependence of the crystallization rate and also to a steplike increase in the crystallinity. The results of SAXS experiments show that the formation of P1b crystallites is governed by the same general laws as for other polymers studied before. Both the crystallization temperature, T_c, and the melting temperature, T_f, are linearly dependent on the reciprocal crystalline layer thickness, d_c^{-1}, but with different slopes and different limiting temperatures for $d_c^{-1} \rightarrow 0$. The observations are again indicative for a crystal development in two steps: First an initial form appears which then transforms into the final lamellar crystallites. As a new feature, in direct correspondence to the two different crystallization mechanisms observed microscopically, two different crystallization lines (d_c^{-1} vs T_c) show up, indicating the occurrence of two different initial states. On the other hand, only one common melting line (T_f vs d_c^{-1}) is found, which means that the two crystallization mechanisms produce crystallites with similar surface free energies. We discuss the peculiar crystallization properties of P1b by comparing the radius of gyration R_g of the chains in the melt with the crystal thickness d_c and propose that the change in the crystallization mechanism could be due to a change from folded-chain to chain-extended crystallization, taking place when d_c gets larger than R_g.

1. Introduction

Poly(1-butene) (P1b) has outstanding mechanical properties. However, its applications are limited compared to those of the lighter olefin polymers such as polyethylene and polypropylene. One main reason is the complication introduced by crystal structure transformations. P1b is polymorphous, with a hexagonal form I and a tetragonal form II as the most common structures. Form I is stable and form II is metastable, but despite the metastability it is always form II which is obtained when P1b crystallizes from the melt. The transformation to form I then takes place after cooling to room temperature, and several days are needed for it.[1−4]

In previous work, we have carried out investigations on syndiotactic polypropylene,[5] polyethylene, poly(ϵ-caprolactone),[6] and isotactic polypropylene[7] for an understanding of the molecular processes involved in the formation of polymer crystallites. Data derived from SAXS experiments yielded the relationships between the crystallization temperature T_c, the melting point T_f, and the crystal thickness d_c at T_c and T_f. In all cases we found two independent linear relations: a "crystallization line" d_c^{-1} vs T_c and a "melting line" d_c^{-1} vs T_f. The occurrence of two separate lines suggests that polymer crystallization takes place in two steps, with an initial state at the beginning and the lamellar crystallite at the end. AFM images indicated that the initial state might be a granular crystalline layer, being composed of crystal blocks with nanometer edge lengths in planar assemblies.

We now looked for the crystallization behavior of P1b, and it turned out as representing a particularly interesting system. Observations in polarized light microscopy, with which we started, showed a change in the crystal morphologies, from spherulites to large quadratic single-crystal-like "hedrites", within a narrow temperature range. Carrying out more experiments (dilatometry, AFM, SAXS), we made an attempt to understand the nature of the phenomenon.

2. Experimental Section

2.1. Samples. Three samples of poly(1-butene) with different molecular weights were investigated. "P1b2", with a weight-average molar mass $M_w = 185\,000$, was purchased from Acros Organics Co. The two other samples, "P1b1" and "P1b3", are commercial products from Montell; weight- and number-averaged molecular weights are $M_w = 141\,000$, $M_n = 40\,000$

† Sichuan University.
‡ Fakultät für Physik der Albert-Ludwigs-Universität.
§ Institut für Makromolekulare Chemie der Albert-Ludwigs-Universität.

10.1021/ma0015875 CCC: $20.00
Published on Web 03/10/2001

for P1b1 and $M_w = 380\,000$, $M_n = 87\,000$ for P1b3. All the molecular weight data were obtained by high-temperature GPC.

2.2. Instrumentation. A polarized light microscope was used together with a home-built heating stage to observe the morphological developments. The morphology at higher resolutions, as it appears at the surface of samples with thicknesses in the micrometer range, was studied by an atomic force microscope ("Nanoscope III") employing the tapping mode.

Crystallization kinetics were registered with a mercury-filled dilatometer. The final weight fraction crystallinities were derived from the total change in the specific volume, by calculating the ratio to the ideal value. For P1b, Δv_{id} is 0.039 cm^3/g.[8]

The SAXS experiments were carried out with the aid of a Kratky camera attached to a conventional Cu Kα X-ray source, employing a temperature-controlled sample holder. Scattering curves were usually registered within 10−20 min counting time, with the help of a position-sensitive metal wire detector. The slit-smeared data were deconvoluted by application of an algorithm developed in our group.[9] Before starting an isothermal crystallization, samples were kept at 170 °C for 20 min to destroy the thermal history and then cooled in the sample holder as fast as possible to the crystallization temperature. By observing the intensity, it was ensured that crystallization did not start before reaching isothermal conditions.

The wide-angle X-ray scattering experiments (WAXS) were conducted using a Siemens D500 diffractometer.

2.3. SAXS Data Analysis. The evaluation of the SAXS patterns was carried out assuming that the stacked lamellae have large lateral dimensions. Then it is possible to derive information on the one-dimensional electron density variation $\rho_e(z)$ along the direction normal to the lamellar surfaces. Scattering intensities can be related to the associated electron density correlation function $K(z)$, defined as

$$K(z) = \langle(\rho_e(z) - \langle\rho_e\rangle)(\rho_e(0) - \langle\rho_e\rangle)\rangle = \langle\rho_e(z)\,\rho_e(0)\rangle - \langle\rho_e\rangle^2$$

and its second derivative $K''(z)$, which gives the interface distance distribution function

$$K''(z) = \frac{O_{ac}}{2}\Delta\rho_e{}^2[h_a(z) + h_c(z) - 2h_{ac}(z)...]$$

h_a, h_c, and h_{ac} denote the distributions of the thicknesses of the amorphous and the crystalline layers and of the long spacings, respectively; O_{ac} is the specific internal surface, i.e., the area per unit volume of the interface separating crystalline and amorphous regions. $\Delta\rho_e$ is the difference of the electron densities of the crystal and the amorphous phase. Both $K(z)$ and $K''(z)$ can be directly calculated by applying Fourier transformations on the scattering intensity distribution $\Sigma(q)$.[10,11]

For two-phase systems the asymptotic behavior of $\Sigma(q)$ can be described by Porod's law

$$\lim_{q\to\infty}\sum(q) = r_e{}^2\,\frac{P}{(q/2\pi)^4}$$

The Porod coefficient P is directly related to O_{ac} by

$$P = \frac{1}{8\pi^3}O_{ac}\Delta\rho_e{}^2$$

P shows also up in the slope of the triangular part of $K(z)$ as

$$P = \frac{1}{4\pi^3}\frac{dK}{dz}$$

3. Results

3.1. Crystal Morphology. Our work on P1b was initiated by observations of the crystallization in a polarized light microscope. We begin with sample P1b1. When carrying out the crystallization isothermally at different temperatures T_c above 80 °C, one finds a total change in the morphology. Figure 1 displays images of structures as they develop at three T_c's. For $T_c = 85$ °C one observes spherulites, but then, at higher temperatures, the appearance changes, and large quadratic crystals are formed. They look like "single crystals", having a uniform chain orientation perpendicular to the surface of the glass slide. Probably the objects are multilayers setup of equally oriented crystallites, and we therefore shall address them in the following as

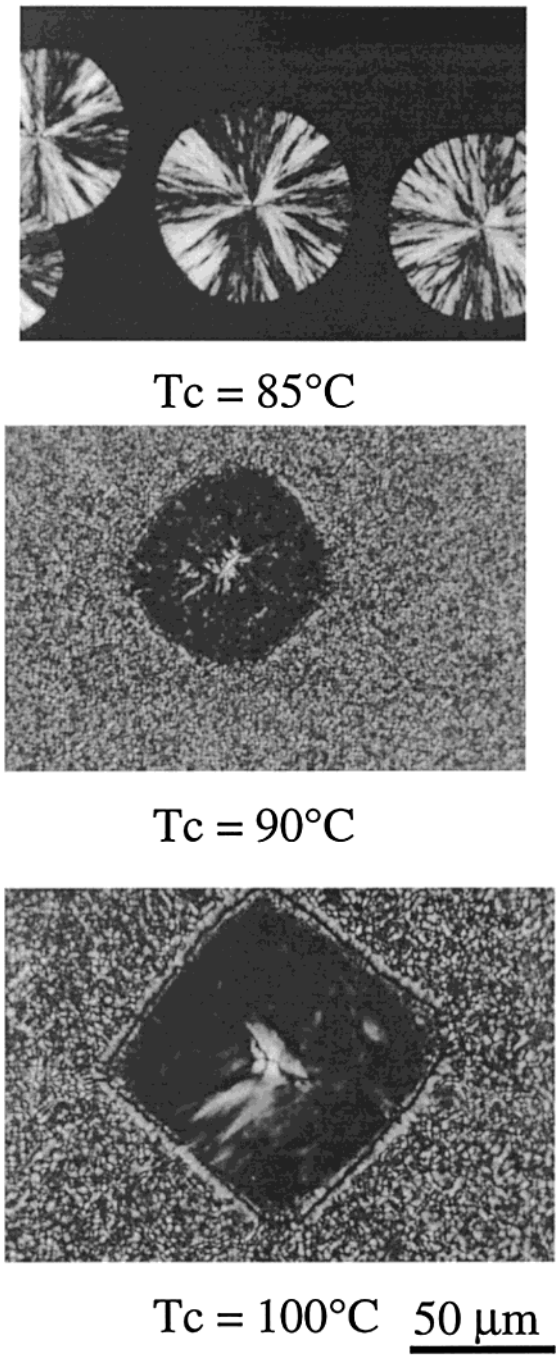

Figure 1. P1b1: morphology development at the indicated temperatures as seen in a polarized light microscope. The picture for $T_c = 85$ °C was obtained at this temperature. The pictures of the structures at 90 and 100 °C were taken after a rapid cooling to room temperature, thus providing a contrast between the nonbirefringened quadratic single crystals and the background of tiny spherulites.

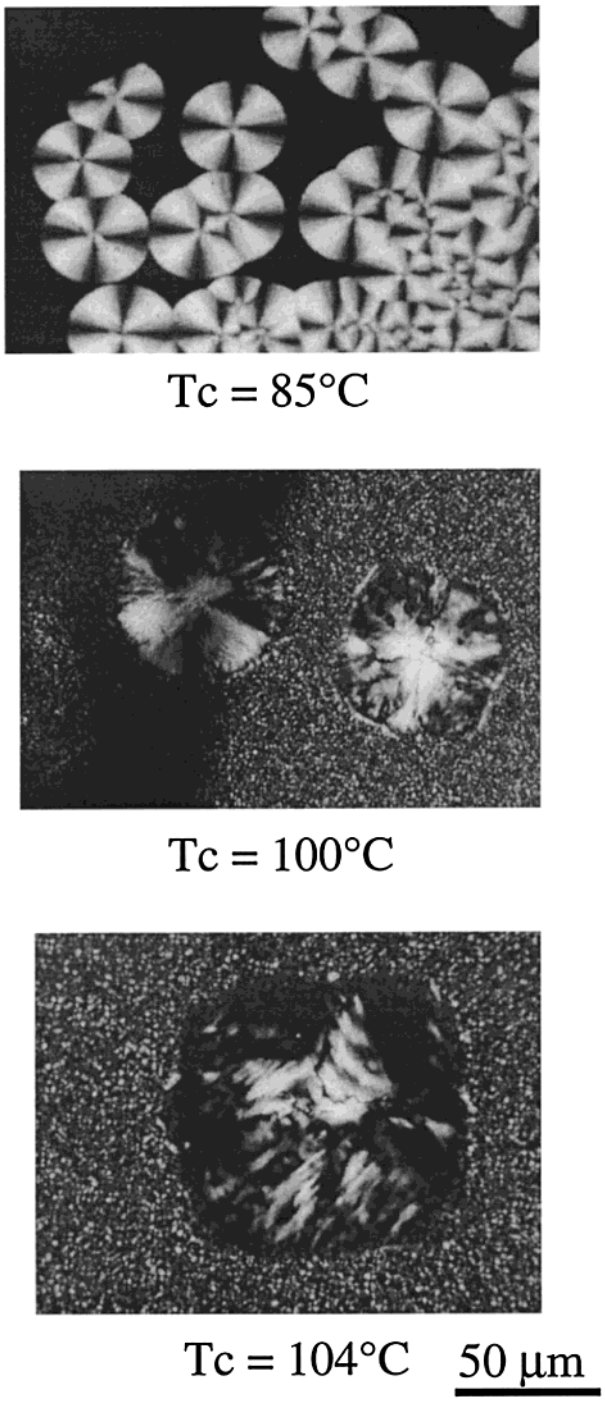

Figure 2. P1b2: morphology formed at the indicated crystallization temperatures. The pictures for 100 and 104 °C were taken after a rapid cooling to room temperature.

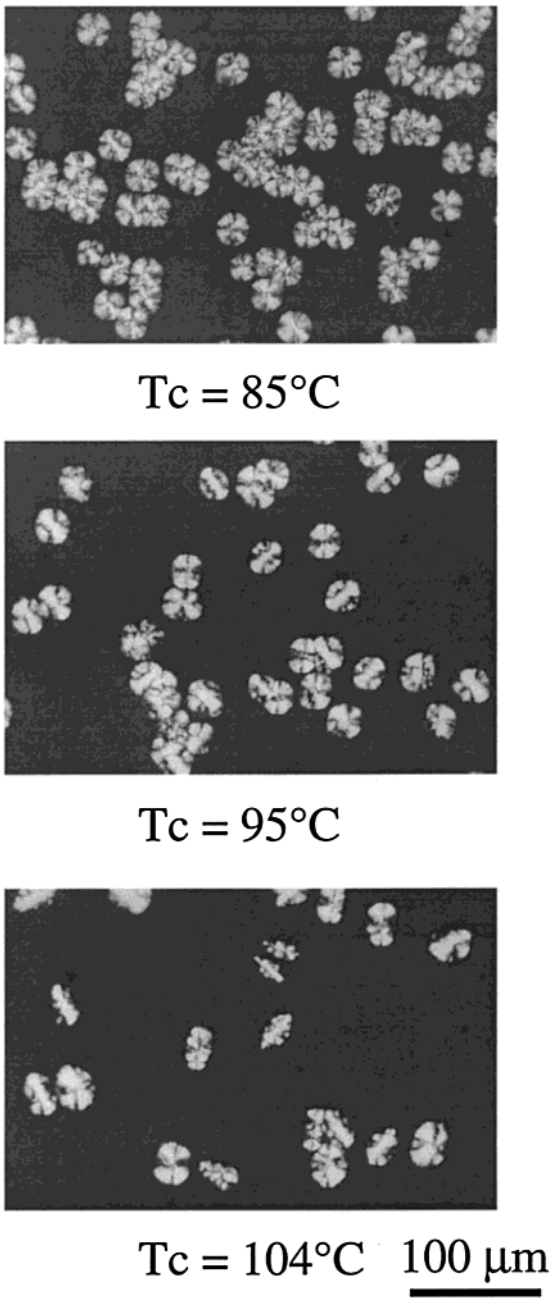

Figure 3. P1b3: morphology developing at the indicated crystallization temperatures.

"hedrites". Different from the picture for T_c = 85 °C, which was obtained at this temperature, the pictures for T_c = 90 and 100 °C were taken after a cooling to room temperature. Without the cooling, which produces many tiny spherulites in the so far not crystallized melt, the single crystals remain nearly invisible.

Figure 2 shows the corresponding observations for sample P1b2. One finds the same morphological transition, now shifted to somewhat higher temperatures. In this case we have at the transition temperature T_c = 100 °C even a coexistence of the two morphologies, i.e., spherulites and hedrites at once.

For sample P1b3, the one with the highest molar mass, no morphological transition is found. Figure 3 shows the structures in the same temperature range, and they are all spherulitic. Hence, the morphological transition is not only temperature-dependent but also molecular weight-dependent. For sample P1b1, having the lowest molecular weight, the change from spherulites to single crystals takes place around 90 °C and for sample P1b2 at 100 °C, whereas for sample P1b3 only spherulites are seen up to 104 °C.

Clearly the morphological transition reflects a change in the mechanism of crystallization, and one has to ask about its nature. To learn about it, we carried out additional experiments: (i) measurements of WAXS curves in order to check whether the morphological transition is accompanied by a change in the crystal structure; (ii) AFM studies to see the morphological change at a higher resolution; (iii) dilatometric measurements to probe for possible associated changes in the crystallization rate and the final crystallinity; (iv)

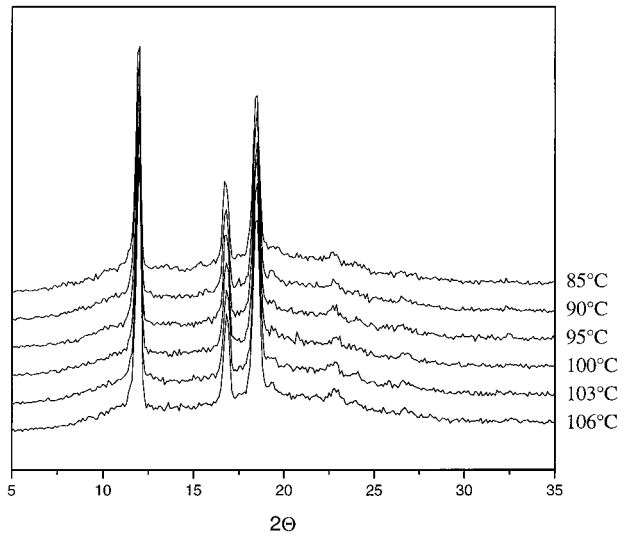

Figure 4. P1b2: WAXS diagrams obtained after completion of isothermal crystallizations at the indicated temperatures (Θ: Bragg scattering angle).

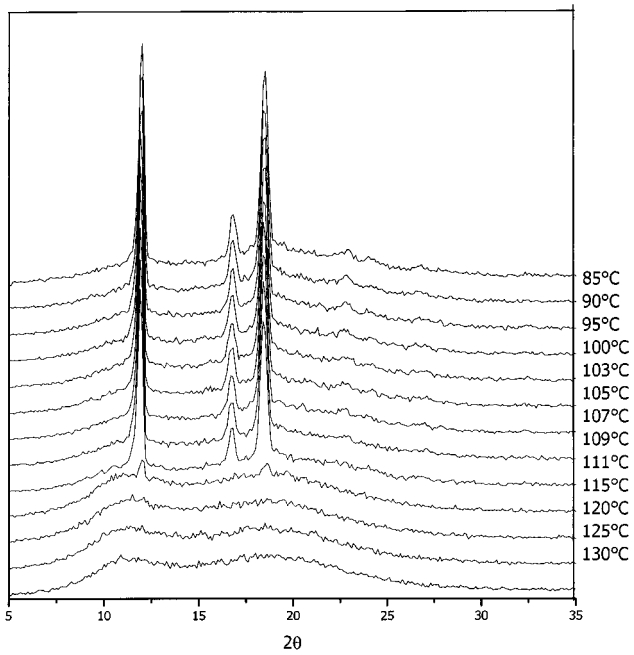

Figure 5. P1b2: WAXS diagrams obtained during heating after an isothermal crystallization at 85 °C.

SAXS investigations to determine crystal thicknesses and long spacings for both morphologies.

3.2. Crystal Structure from WAXS. P1b crystals can exist either in the metastable form II (tetragonal) or in the stable form I (hexagonal). Both have characteristic scattering patterns which are known from the literature. We carried out WAXS experiments in the temperature range of our investigations. Figure 4 shows WAXS curves for sample P1b2. One observes always, at all crystallization temperatures, crystal form II, which is characterized by three typical peaks, located at $2\Theta = 12°$, 17°, and 18.5°. Hence, the observed change in the crystallization mechanism takes place for a constant crystal structure.

A heating subsequent to the crystallization does not change the structure. As an example, Figure 5 depicts the WAXS curves of P1b2 after being crystallized at 85 °C.

3.3. AFM Observations. To obtain a more detailed insight, we carried out an AFM experiment for sample P1b2. We chose two crystallization temperatures: one in the low-temperature range, $T_c = 85$ °C, and one in the high-temperature range, $T_c = 104$ °C. The crystallized samples were cooled to room temperature and then investigated. Images are shown in Figure 6 and Figure 7. They obviously correspond to the optical micrographs. For $T_c = 85$ °C images show stacks of layerlike crystallites, as parts of spherulites, mostly in edge-on views. On the other hand, for samples crystallized at $T_c = 104$ °C laterally extended, uniformly flat-on oriented lamella are observed. Hence, the morphology, as given by the sizes and the orientational distribution of the lamellae, is not affected by the transition from form II to form I, which, although slowly, takes place at room temperature. The AFM images yield an estimate of the long period and the crystal thickness. For $T_c = 85$ °C, the long period is about 30 nm, and crystal lamella have a thickness of about 15 nm; at $T_c = 104$ °C, the long period is about 42 nm, and the crystal thickness is about 27 nm.

Generally, lamellae show a granular substructure. The observation is not new. Studying similarly treated, i.e., at elevated temperatures isothermally crystallized and then cooled samples, Geil et al.,[12] employing dark field electron microscopy, also found a blocky substructure. It developed and became visible during storage at room temperature, directly related to the slow transition from form II to the stable form I.

3.4. Dilatometric Registration of Crystallization Kinetics. Since the crystallization process was slow, dilatometry was used to investigate the kinetics and furthermore to determine the crystallinities found at the end of isothermal crystallizations. We carried out such experiments for the samples P1b1 and P1b2. Figure 8 depicts for sample P1b1 the decrease of the specific volume Δv with time as measured at the indicated temperatures. Curves show a systematic shift along the log t axis. One also observes an increase of the total drop of the specific volume, from 0.018 to 0.021 cm^3/g, when the crystallization temperature changes from 75 to 100 °C. Figure 9 gives the results for sample P1b2. The total drop in the specific volume is 0.019 cm^3/g within the temperature range of the spherulites (85−95 °C), and $\Delta v = 0.023$ cm^3/g in the range of the hedrites (above 100 °C). We conclude from these data that the change in the crystallization mechanism results also in a different crystallinity. For the spherulites we have $\phi \approx 0.019/0.039 \approx 0.5$, and for the hedrites $\phi \approx 0.023/0.039 \approx 0.6$.

One finds also effects of the morphological transition on the crystallization rate. Figures 10 and 11 show the temperature dependencies of the half-time of crystallization τ for the two samples. For sample P1b2 the transition is accompanied by a break, leading to a more sensitive temperature dependence of τ for the hedrites. The properties of sample P1b1 are basically similar, but the transition occurs in a smooth manner.

3.5. Time- and Temperature-Dependent SAXS Experiments. To see the development of the crystallites during the crystallization and their melting during a subsequent heating, one has to carry out time- and temperature-dependent SAXS experiments. They yield the crystal thickness and the long spacing. For P1b SAXS experiments are principally difficult. The electron density difference $\Delta\rho_e$ which controls the scattering

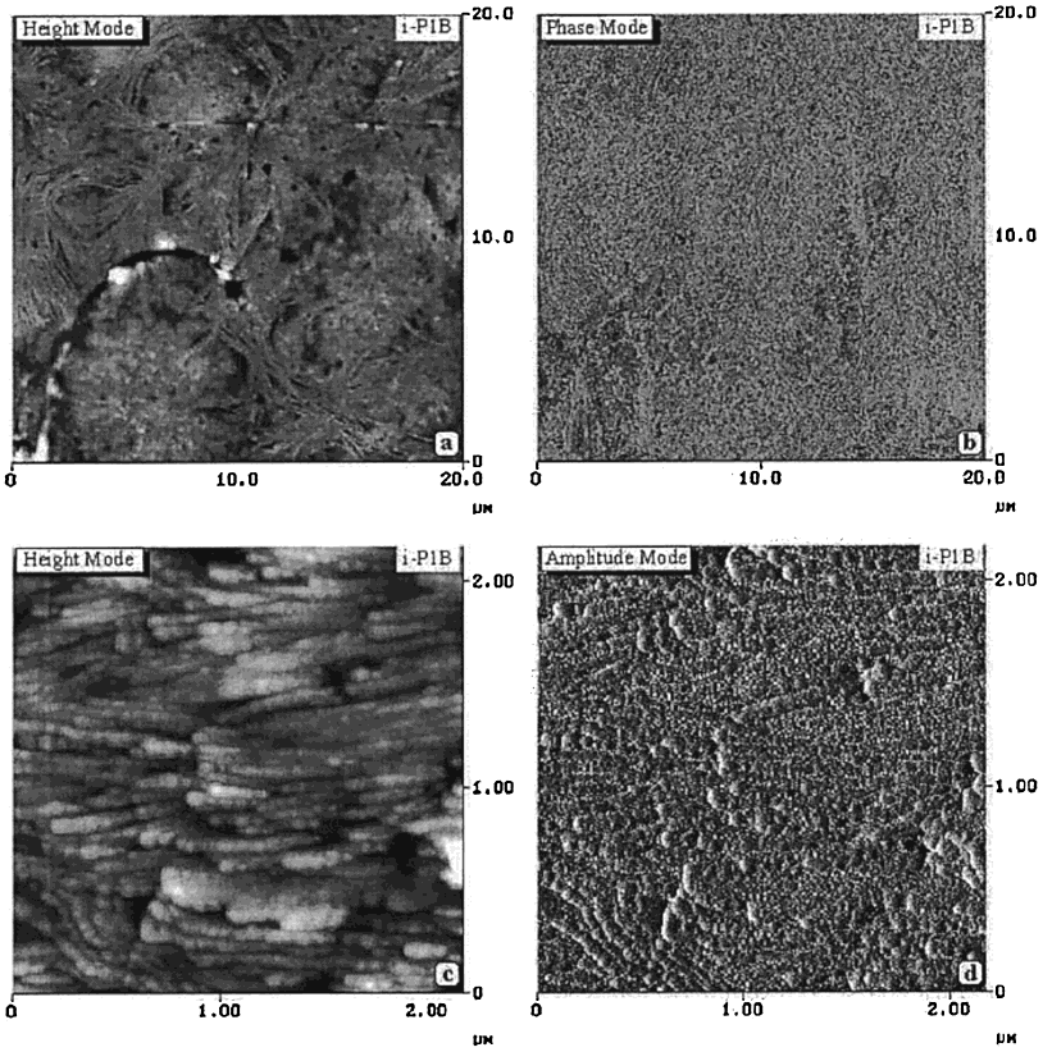

Figure 6. P1b2: AFM images obtained at room temperature after an isothermal crystallization at 85 °C.

intensity is very low, 5 times smaller than, for example, for polyethylene. SAXS intensities, being proportional to $(\Delta\rho_e)^2$, are therefore more than 1 order of magnitude below those of other standard polymers. We could not expect, therefore, to obtain results with the same degree of precision as for other investigated systems; however, as will be shown, they are still clear in the basic features.

We base, as in previous studies, the analysis on the interface distance distribution function $K''(z)$, from which one can derive the most probable thicknesses of the crystals and amorphous layers. Results varied in quality; there were clear cases and others with rather large error limits. Figures 12−16 give some selected results and demonstrate the given situation. Figure 12 and Figure 13 represent favorable cases. They concern sample P1b2 and show in the lower parts the evolution of the interface distance distribution function during isothermal crystallizations at a temperature in the spherulite range, $T_c = 85$ °C, and at a temperature in the hedrite range, $T_c = 104$ °C. The upper parts refer to the structure variations during a subsequent heating, showing on the left the changes in $K''(z)$ and on the right-hand side the simultaneous changes of the Porod coefficient. For $T_c = 104$ °C, two peaks located around 14 and 27 nm are seen. The minimum in $K''(z)$, corresponding to the long spacing L, is at 41 nm. Since the crystallinity is above 0.5, as deduced from dilatometry, the assignment is clearly $d_a \approx 14$ nm and $d_c \approx 27$ nm. This gives a linear crystallinity $\phi_l = d_c/L \approx 0.65$, in rough agreement with the dilatometer value. Only one peak is seen for $T_c = 85$ °C. This peak is located at 14 nm, and the long spacing is 28 nm. So the peak assignment is 14 nm for both d_a and d_c, which gives for the spherulites a linear crystallinity $\phi_l \approx 0.50$, again in agreement with the dilatometric result. To show the changes of the lamellar structure through the morphological transition, Figure 14 collects the curves $K''(z)$ obtained for sample P1b2 after completion of isothermal crystallizations at the different temperatures. The curves show one prominent peak for $T_c < 95$ °C and two peaks in $K''(z)$ for $T_c > 100$ °C, i.e., more generally speaking, a change from a one-peak to a two-peak appearance when T_c crosses the transition range (the peak at 4 nm is an artifact of unknown origin). In the transition range $T_c = 95-100$ °C, one might even see the three peaks expected from the PLM image in Figure 2 with the coexistence of two kinds of crystal lamellae at one crystallization temperature.

It is evident that the crystal thickness remains constant during the isothermal crystallization process, for both $T_c = 104$ °C and $T_c = 85$ °C. This was indeed true for the whole temperature range studied. As shown in the upper parts of Figures 12 and 13, $K''(z)$ curves vary during the subsequent heating. At the beginning, one observes only an increase in P, as expected due to

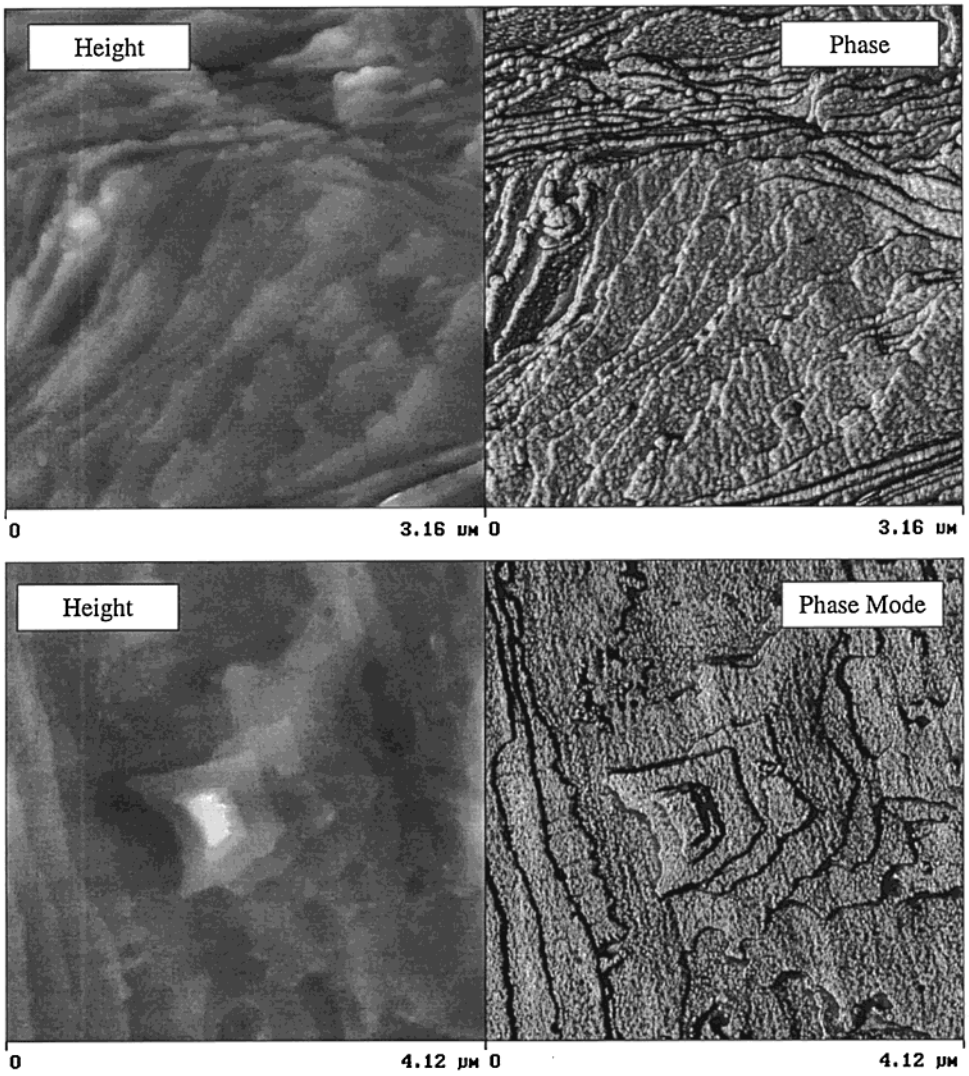

Figure 7. P1b2: AFM images obtained at room temperature after an isothermal crystallization at 104 °C.

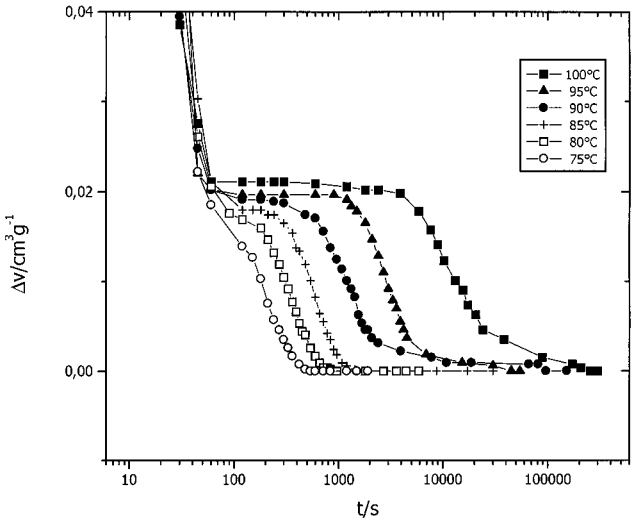

Figure 8. P1b1: kinetics of isothermal crystallization at the indicated T_c's followed by dilatometry.

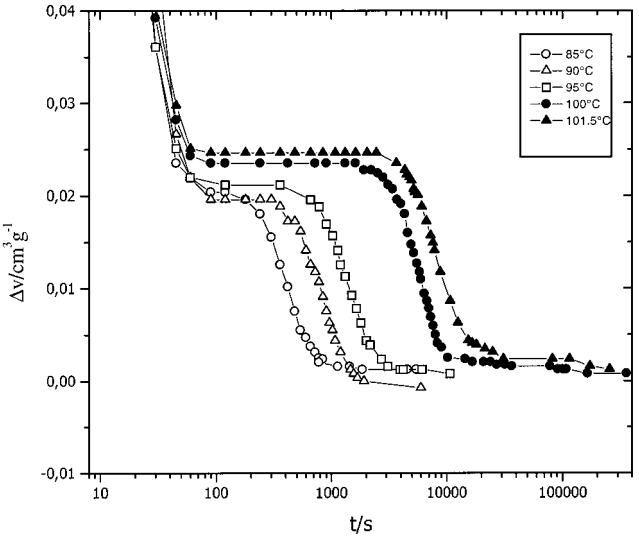

Figure 9. P1b2: kinetics of isothermal crystallization at the indicated T_c's followed by dilatometry.

the increase of the electron density difference with temperature. From a certain temperature upward, P gets constant or decreases, which indicates a melting, and some degrees higher a shift of d_c is observed indicative for recrystallization processes. For the sample crystallized at $T_c = 85$ °C, the shifting of d_c occurs at 103 °C; the complete disappearance of $K''(z)$, corresponding to the final melting, takes place at $T_f = 113$ °C, at a crystal thickness $d_c = 23$ nm. In the sample crystallized at 104 °C the crystallites are more stable. First shifts of d_c show up around $T_f = 112$ °C. At 116

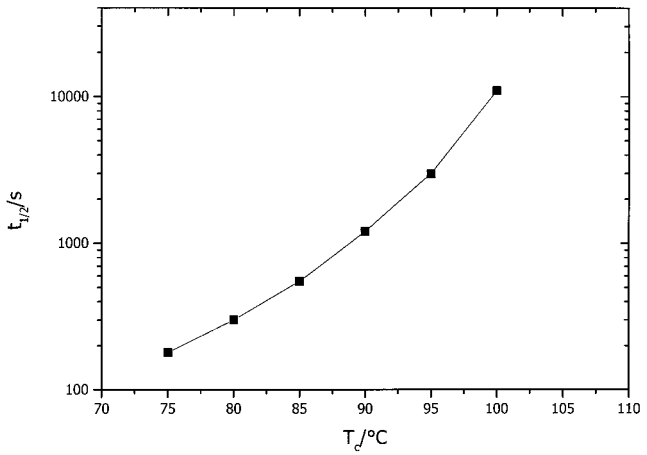

Figure 10. P1b1: half-time of crystallization as a function of T_c derived from Figure 8.

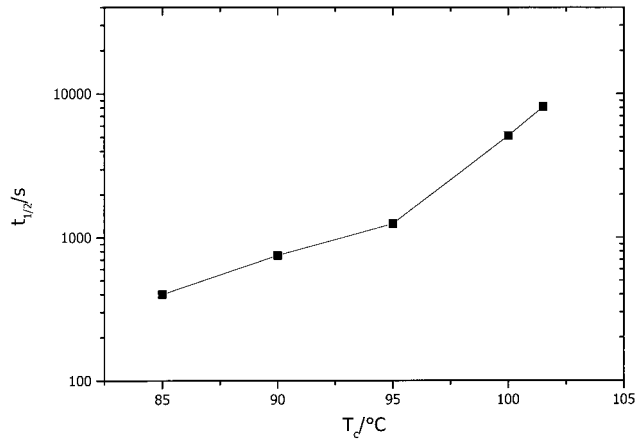

Figure 11. P1b2: half-time of crystallization as a function of T_c derived from Figure 9.

°C, the final melting, d_c has increased to 34 nm.

As an example for K'' curves obtained for sample P1b1, Figure 15 gives the result of an experiment at T_c = 100 °C. Two peaks, located at 14 and 23 nm, are seen. The minimum of the long spacing is at 37 nm. The peak assignment is again clear. We have $d_a \approx 14$ nm and $d_c \approx 23$ nm, which gives a linear crystallinity $\phi_l \approx 0.62$, comparable to the dilatometric result. As for sample P1b2, the crystal thickness keeps constant during the isothermal crystallization process. A difference is seen during the subsequent heating: there is no indication for melting−recrystallization processes, up to 112 °C. Obviously crystallites are just removed from the stack. As the removal of one crystallite leads to the disappearance of two amorphous layers, it is clear why the effect on the d_a peak is stronger than for the d_c peak.

Figure 16 refers to sample P1b3 with the highest molecular weight and shows K'' curves, which were obtained for an isothermal crystallization at T_c = 104 °C. There are larger fluctuations in the data, and there is again an artificial peak near the origin; however, the general form seems still clear: One finds a peak at around 22 nm and a minimum, giving the long spacing, at around 44 nm. This gives a crystallinity around 0.5, which indeed is that associated with the spherulites.

What do we learn from the SAXS analysis? Despite the uncertainties resulting from the low scattering intensities, we can draw some definite conclusions: The change in the crystallization mechanism is associated

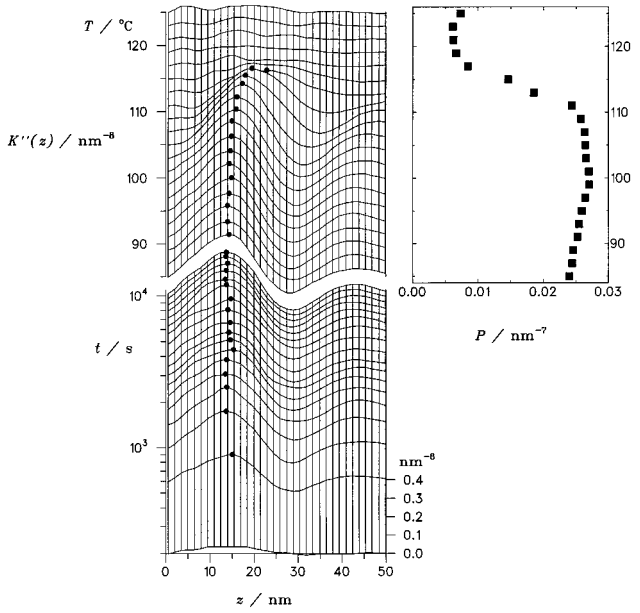

Figure 12. P1b2: evolution of the interface distance distribution function $K''(z)$ during an isothermal crystallization at 85 °C (bottom left) and changes during a subsequent heating to the melt (top left). Related changes of the Porod coefficient (top right).

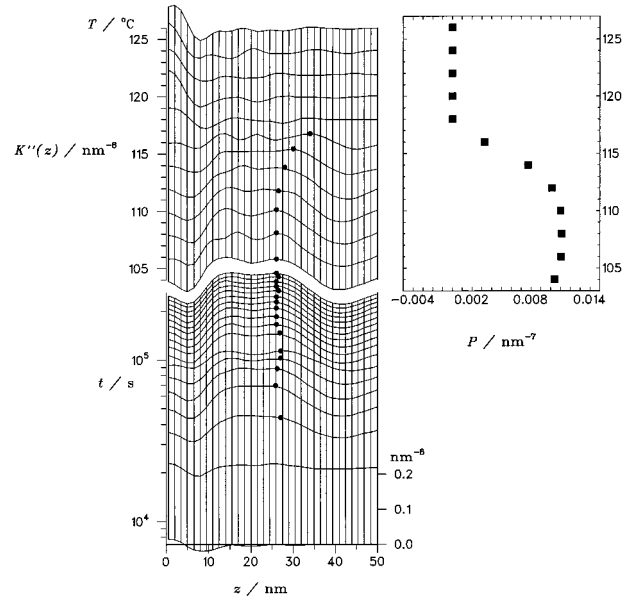

Figure 13. P1b2: evolution of the interface distance distribution function $K''(z)$ during an isothermal crystallization at 104 °C and changes during a subsequent heating to the melt. Related changes of the Porod coefficient.

with steplike changes in both the crystal thickness and the long spacing. Furthermore, together with the dilatometrically determined volume fraction crystallinity also the linear crystallinity ϕ_l changes to higher values when passing from spherulites to the hedrites.

3.6. Crystallization Lines and Melting Lines. A main finding in previous crystallization studies by SAXS was the observation of a crystallization line and a melting line (T_c and T_f vs d_c^{-1}) as two independent dependencies. The data now obtained for P1b again allow us to probe these relationsships. We collected all the d_c values measured for the three samples at different crystallization temperatures and looked also for the crystal thicknesses of the melting points T_f. Figure 17

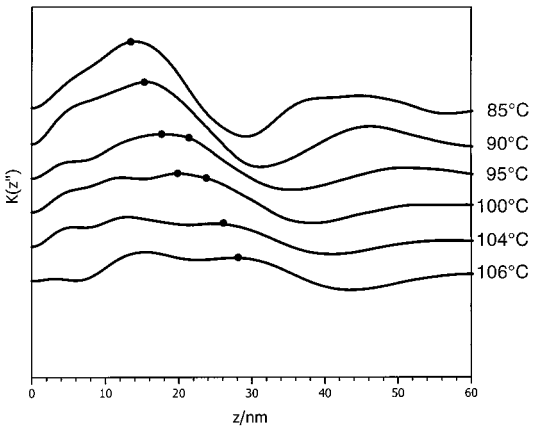

Figure 14. P1b2: interface distance distribution function derived from SAXS curves obtained after completion of isothermal crystallizations at the indicated temperatures.

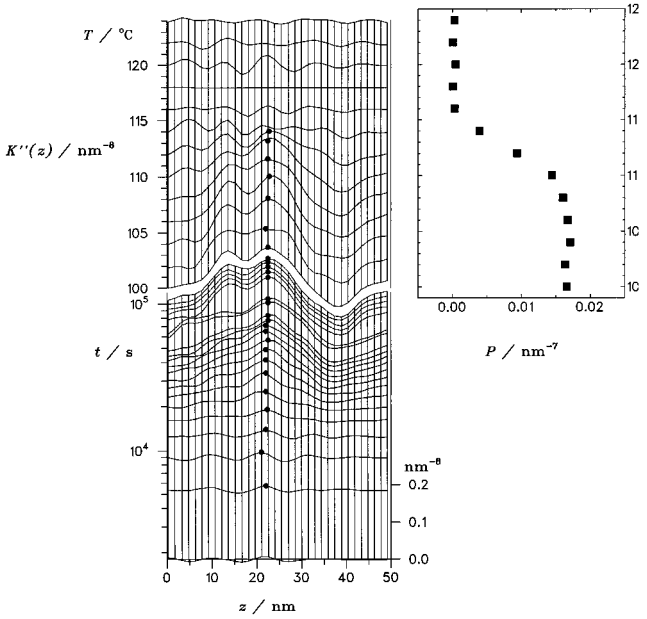

Figure 15. P1b1: evolution of the interface distance distribution function $K''(z)$ during an isothermal crystallization at 100 °C and changes during a subsequent heating to the melt. Related changes of the Porod coefficient.

presents the results in one common plot for all three samples. The open symbols refer to the relation T_c vs d_c^{-1}. As for all other polymers studied, one finds also for P1b a linear dependence. Peculiar for P1b, originating from the two crystallization mechanisms one observes here two crystallization lines. They look indeed straight and, as it appears, extrapolate for $d_c \rightarrow \infty$ to the same limiting temperature, $T_c^{\infty} \approx 136$ °C. The line associated with the hedrites has a larger slope than the spherulite-crystallization line.

The two lines are not molecular weight dependent. As long as the crystallization takes place by the same mechanism, data fall on the same line. One observes for sample P1b2 data on the spherulite-crystallization line, when T_c is below 95 °C, and on the hedrite-crystallization line, when T_c is above 100 °C. In the transition range 95−100 °C, two d_c's are seen, one on each line. For the higher molecular weight sample P1b3 the measured d_c's are located on the spherulite-crystallization line only.

The filled symbols in Figure 17 give the melting points. The Gibbs−Thomson law predicts a linear

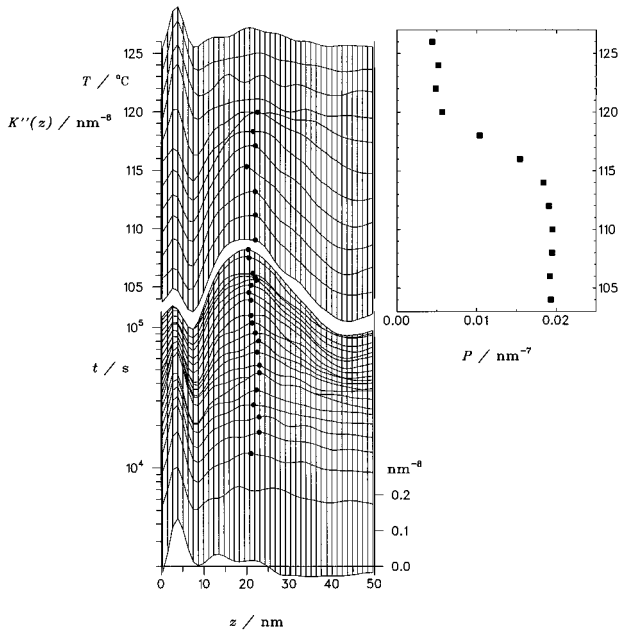

Figure 16. P1b3: evolution of the interface distance distribution function $K''(z)$ during an isothermal crystallization at T_c = 104 °C and changes during a subsequent heating to the melt. Related changes of the Porod coefficient.

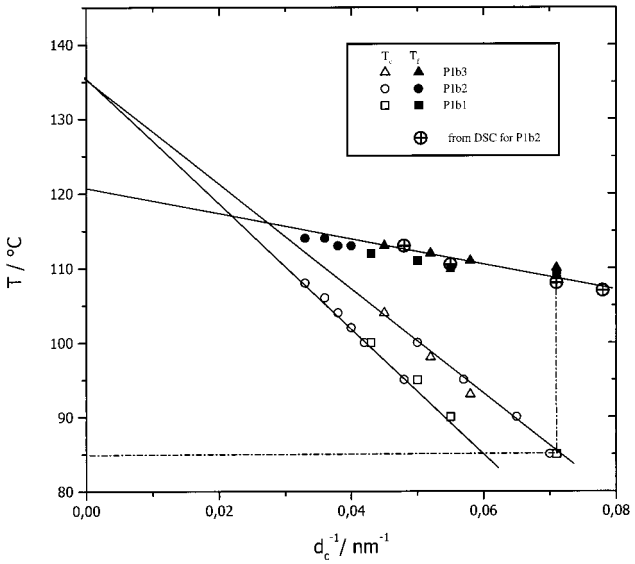

Figure 17. P1b1, P1b2, and P1b3: crystallization lines T_c vs d_c^{-1} and melting lines T_f vs d_c^{-1} as derived from the time- and temperature-dependent SAXS experiments. Comparison with DSC melting points measured for P1b2.

relationship between T_f and d_c^{-1} for layerlike crystallites. When examining this dependence, it is necessary to check whether and where a melting−recrystallization occurred during the heating. The determination of melting points for sample P1b1 and P1b3 was simple, because there was no recrystallization. For sample P1b2 we had indications for a melting−recrystallization process. In this case, we took the temperature at which the $K''(z)$ peak completely disappeared as the melting temperature, together with simultaneously measured values of d_c. Corresponding to two crystallization lines, one might expect to find two melting lines as well, because two different mechanisms should in general produce lamellae with different surface free energies. As a matter of fact, within the error limits of the data we only observed one melting line. All points in Figure

17 are located on it; there is no difference among the three samples. Of course, there still may exist two melting lines, but then the difference of surface free energies produced by the two mechanism is too small to be detectable by our experiments. The melting line extrapolates toward the equilibrium melting point, and we find $T_f^\infty \approx 121$ °C. Figure 17 includes also three melting points obtained by DSC for sample P1b2, in the range of both lower and higher temperatures. They were plotted as indicated by the arrow, which refers to a crystallization at 85 °C and agree with the SAXS results.

Hence, as demonstrated by Figure 17, P1b obeys the same general laws as the previously studied other system. As indicated by the existence of crystallization lines independent from the Gibbs−Thomson melting line, for this polymer the building up of the lamellar crystallites again takes place via a route over intermediate states.

4. Discussion

4.1. Chain Disentangling as Cause of the Spherulite−Hedrite Transition? Why do we observe two morphologies and crystalline lines, indicative for a change in the mechanism of crystallization for P1b, here for the first time, and not for the other polymers in our previous work? On the basis of the observed molecular weight dependence of the temperature of morphological transition, we give in the following a hypothetical answer. We study here, as in the previous investigations, crystallizations out of entangled polymer melts which result in layerlike crystallites embedded in and coupled by the fluid matrix. In principle, the crystallization does not necessitate a chain disentangling. The entanglements are just shifted into the amorphous regions, where they become accumulated together with the other noncrystallizable chain parts like end groups, counits, and stereodefects. The volume occupied by the chains remains unchanged. This was demonstrated by Schelten et al. by neutron scattering experiments[13] and then led Fischer to formulate his "solidification model" where the formation of the crystalline−amorphous layer structure occurs by local processes only.[14] This situation, however, has a prerequisite: The crystal thickness has to be smaller than the diameter of the volume occupied by the chains in the melt. An estimate for this diameter is the radius of gyration R_g. We therefore have the condition

$$d_c < R_g$$

What happens if it is not fulfilled, i.e., if the crystal thickness as determined by the kinetical pathway followed by the crystallization process surpasses the radius of gyration of the chain in the melt? Obviously the chains will then begin to disentangle. The consequence might be a change in the crystallization mechanism leading to another form of crystallites, the one sometimes addressed as "chain-extended". Exactly this is our suggestion: Could not it be that the morphological transition observed for P1b represents a change from folded-chain to chain-extended crystallites, i.e., that the spherulites grow without any disentangling, whereas the hedrites represent a form that requires some disentangling?

To check the idea, we compare R_g and d_c values. R_g and the mean-squared end-to-end distance R_0 are for Gaussian chains related by

$$R_g^2 = \frac{R_0^2}{6}$$

and R_0 can be calculated using the characteristic ratio C_∞ as

$$R_0^2 = C_\infty a_b^2 N$$

Here, a_b^2 stands for the sum of the squares of the lengths of the backbone bonds of one monomer unit, and N is the degree of polymerization. We find in the literature for P1b $C_\infty = 18$,[8] which in fact is an unusually high value; a_b^2 is 4.74×10^{-2} nm^2. The values calculated for our samples for R_g are shown in Table 1. To check also the situation for other studied systems, s-PPs and copolymerized PEs, the table includes also values of R_g and d_c for these samples.

Table 1. Values of the Radius of Gyration R_g of Polymers under Study

sample	M_w (g mol^{-1})	C_∞	a_b^2 (nm^2)	R_g (nm)	d_c range (nm)
P1b 1	141 000	18	4.74×10^{-2}	18.9	14−24
P1b 2	185 000			21.6	14−30
P1b 3	380 000			31.0	14−21
P(E-*co*-O)7	87 360	6.8	4.74×10^{-2}	11.9	5.5−7
P(E-*co*-O)14	90 600			11.1	4.5−6.6
s-PP	176 800	6.2	4.74×10^{-2}	14.3	6.6−10
s-PP(P-*co*-O)4	153 300			12.7	5.8−8.3
s-PP(P-*co*-O)15	159 800			11.9	3.7−5
s-PP(P-*co*-O)20	99 200			9.2	3−4.2

As we see, the comparison between R_g and d_c indicates that our idea could be right. For P1b3, R_g is 31 nm, clearly above the crystal thickness at all temperatures, and we indeed have spherulites throughout. For P1b1 and P1b2 we find a different situation; R_g is in the middle of the range of the observed d_c values. For the spherulites we have $d_c < R_g$. The jump in the thickness associated with the transition to the hedrites then leads to values (18 and 22 nm) which happen to essentially agree with R_g.

Also, the results for sPP and PE, where we observed spherulites only, agree with our suggestion. The values of the radius of gyration for these samples as given in the table are always clearly larger than the crystal thicknesses. Under this condition we indeed expect a uniform spherulitic crystallization mechanism.

Hence, it appears to be possible that the P1b spherulites are composed of chain-folded crystallites forming without any disentangling and that the hedrites represent chain-extended crystallites which require for their development some disentangling. Which mechanism occurs then would depend on the crystal thickness when compared to the radius of gyration. One observes a transition when d_c, which generally increases with temperature, reaches values similar to R_g.

4.2. Some Remarks Concerning the Route Followed during the Formation of Polymer Crystallites. For many polymer systems one can obtain either spherulites or large single crystals, depending on the crystallization conditions. This is not the place to review the manifold of observations gathered over many years, but what we want to do is to point at a main question arising from the findings: Is there a qualitative difference between a typical spherulitic melt crystallization and crystallizations from dilute solutions or in thin

films, to cite just two cases which promote the growth of objects with single-crystal texture? Or is the change continuous? In the majority of cases the issue could not be treated. Studies concerned either single crystals, which enable a more detailed structure analysis to be carried out, or spherulites, which are generally looked at in a more global way. Now, for P1b, we have an example where we have both morphologies and a temperature-induced change. It takes place within a narrow range and changes the crystal thicknesses as well as the crystallinity. In fact, the phenomenon looks much more like a transition, associated with a change in the crystallization mechanism, than a smooth variation. Hence, P1b could give an answer to the question, one in favor of a qualitative difference between the mechanism of spherulite growth and that leading to single crystals. In the tentative explanation presented in the previous section we relate the change with the onset of disentangling processes. The time required for a disentangling will depend on the local mobility; however, whether a disentangling is necessary at all may well be determined by a structural property only, namely, as proposed, on the ratio between the crystal thickness and chain diameter in the melt.

In a recent paper experimental evidence was collected, which speaks in favor of a route over transient states when crystals form out of an entangled melt.[15] A specific route was proposed which can explain the observations. The first step therein is the creation of a mesomorphic layer. This layer spontaneously thickens, up to a critical value, where it solidifies through a cooperative phase transition. The transition produces a granular crystalline layer, which transforms in the last step into homogeneous lamellar crystallites. A main motivation for setting up this model was the general finding, in all systems investigated so far, of a crystallization and a melting line as two independent features, with different slopes and limiting temperatures. We associate the melting line as usually with the Gibbs−Thomson law of lamellae melting and the crystallization line with the transition from the mesomorphic to the granular crystalline state. The proposed mechanism differs from the widely used Hoffman−Lauritzen[16] model of growth control by secondary nuclei or Sadler's[17] model of entropic barriers, in a basic property: The existing models commonly start from the assumption that crystals grow by a direct attachment of chain sequences from the isotropic melt onto the growth faces. The new experiments contradict this view, by providing evidence in favor of a multistage route, where transient states are passed through when transforming the isotropic melt into the layerlike crystallites.

In the crystallization of P1b discussed in this work we observe again crystallization lines, now two different ones, and the melting line as independent properties. Hence, the change of the crystallization mechanism does not change the multistage character of the route followed in the formation of crystallites. An initial state apparently exists in both cases: the formation of spherulites and hedrites.

One reason for proposing a granular crystalline layer as an intermediate stage on the route to homogeneous lamellar crystallites was the frequent observation of a blockiness of lamellae when carrying out AFM scans on different systems.[18−20] For P1b we find again this substructure; however, in this case it could also arise from the form II to form I transition. Here, additional time-dependent experiments are necessary for a clarification.

5. Conclusion

In summary, we find in P1b a morphological transition from a spherulitic to a hedritic, single-crystal-like structure. The transition temperature is molar mass-dependent. Correspondingly, two crystallization lines are observed. An estimate suggests that the crystallization mechanism changes, when the crystal thickness gets similar to the radius of gyration of the chains in the melt. We therefore interpret the transition as a change from the growth of chain-folded crystallites to the growth of chain-extended crystallites, taking place without or with a partial disentangling, respectively.

Acknowledgment. Support of this work by the Deutsche Forschungsgemeinschaft and by the "Fonds der Chemischen Industrie" is gratefully acknowledged. We express our great thanks to Prof. G. Alfonso (Genova) for providing us with samples and for many helpful discussions. Q.F. would particularly like to express his gratitude to the Alexander von Humboldt-Stiftung and the China National Distinguished Young Investigator Fund for financial support.

References and Notes

(1) Natta, G.; Pino, P.; Corradini, P.; Danusso, F.; Mantica, E.; Mazzanti, G.; Moraglio, G. *J. Am. Chem. Soc.* **1955**, *77*, 1708.
(2) Natta, G. *Makromol. Chem.* **1960**, *35*, 94.
(3) Turner Jones, A. *Polym. Lett.* **1963**, *1*, 455.
(4) Petraccone, V.; Pirozzi, B.; Frasci, A.; Corradini, P. *Eur. Polym. J.* **1976**, *12*, 323.
(5) Hauser, G.; Schmidtke, J.; Strobl, G. *Macromolecules* **1998**, *31*, 6250.
(6) Heck, B.; Hugel, T.; Iijima, M.; Sadiku, E.; Strobl, G. *New J. Phys.* **1999**, *1*, 17.
(7) Iijima, M.; Strobl, G. *Macromolecules* **2000**, *33*, 5204.
(8) Brandrup, J.; Immergut, E. H.; Grulke, E. A. *Polymer Handbook*, 4th ed.; John Wiley & Sons: New York.
(9) Strobl, G. *Acta Crystallogr.* **1970**, *A26*, 367.
(10) Ruland, W. *Colloid Polym. Sci.* **1977**, *255*, 417.
(11) Schmidtke, J.; Strobl, G.; Thurn-Albrecht, T. *Macromolecules* **1997**, *30*, 5804.
(12) Chau, K. W.; Yang, Y. C.; Geil, P. H. *J. Mater. Sci.* **1986**, *21*, 3002.
(13) Schelten, J.; Ballard, B. G.; Wignall, G. D.; Longmann, G.; Schmatz, W. *Polymer* **1976**, *17*, 751.
(14) Fischer, E. W. In *Investigation of the Crystallization Process of Polymers by Means of Neutron Scattering;* Kleintjens, L. A., Lemstra, P. J., Eds.; Integration of Fundamental Polymer Science and Technology; Elsevier: New York, 1986.
(15) Strobl, G. *Eur. Phys. J.* **2000**, *E3*, 165.
(16) Hoffman, J. D.; Davis, G. T.; Lauritzen, J. I. *Treatise Solid State Chem.* **1976**, *3*, 497.
(17) Sadler, D. M. *Nature* **1987**, *326*, 174.
(18) Hugel, T.; Strobl, G.; Thomann, R. *Macromolecules* **1998**, *31*, 6250.
(19) Magonov, S.; Godovsky, Y. *Am. Lab.* **1999**, *31*, 55.
(20) Loos, J.; Thüne, P. C.; Lemstra, P. J.; Niemantsverdriet, W. J. *Macromolecules* **1999**, *32*, 8910.

MA0015875